Tailoring ZSM-5 Zeolites for the Fast Pyrolysis of Biomass to Aromatic Hydrocarbons

Hoff, Thomas C.; Gardner, David W.; Thilakaratne, Rajeeva; Wang, Kaige; Hansen, Thomas Willum; Brown, Robert C.; Tessonnier, Jean Philippe

Published in:
ChemSusChem (Print)

Link to article, DOI:
10.1002/cssc.201600186

Publication date:
2016

Document Version
Peer reviewed version

Tailoring ZSM-5 Zeolites for the Fast Pyrolysis of Biomass to Aromatic Hydrocarbons

Thomas C. Hoff,[a] David W. Gardner,[a] Rajeeva Thilakaratne,[b] Kaige Wang,[b] Thomas W. Hansen,[c] Robert C. Brown,[b] and Jean-Philippe Tessonnier*[a]

Abstract: The production of aromatic hydrocarbons from cellulose by zeolite-catalyzed fast pyrolysis involves a complex reaction network sensitive to the zeolite structure, crystallinity, elemental composition, porosity, and acidity. The interplay of these parameters under reaction conditions represents a major roadblock that has hampered significant improvement in catalyst design for over a decade. Here, we studied commercial and laboratory synthesized ZSM-5 zeolites and combined data from ten complementary characterization techniques in an attempt to identify parameters common to high-performance catalysts. Crystallinity and framework aluminum sites accessibility were found to be critical to achieve high aromatic yields. These findings enabled us to synthesize a ZSM-5 catalyst with enhanced activity, offering the highest aromatic hydrocarbon yield reported to date.

Introduction

The fast pyrolysis of lignocellulosic biomass represents a simple, cheap, and efficient approach to produce bio-based fuels and chemicals from renewable feedstocks.[1] In this process, solid biomass is heated to high temperature (500 – 700 °C) to be thermochemically converted to light gases (CO, CO_2), solid char, and organic vapors, which can be further condensed to obtain the desired liquid bio-oil.[2] The ratio between the gas, liquid, and solid fractions is particularly sensitive to the heating rate. Fast heating rates on the order of 1000 °C/s are required to achieve bio-oil yields of 60 – 70%.[3] The main byproducts are CO, CO_2, and H_2O, which result from decarbonylation, decarboxylation, and dehydration. These deoxygenation reactions are desired as they increase the energy density of the liquid fraction, thus its potential as a biofuel.[4] Fast pyrolysis is also attractive because this versatile technology can accommodate a wide range of feedstocks including wood, switchgrass, and agricultural waste (*e.g.* corn stover). However, bio-oil is a complex mixture of more than 300 oxygenated compounds, namely anhydrosugars, organic acids, aldehydes, ketones, furanics, and phenolics.[5] Its high oxygen content and chemical complexity makes it unsuitable for direct use as a biofuel. Additional processes that involve one or several heterogeneous catalysts are required to decrease the oxygen concentration from ~45% to less than 7% and achieve stable blends with petroleum that allow refining.[6] Various catalytic deoxygenation processes have been investigated and reviewed recently.[7] Integrated approaches where the catalyst is directly mixed with the biomass are appealing as pyrolysis and deoxygenation occur simultaneously in the same reactor. Notably, catalytic fast pyrolysis (CFP) using ZSM-5 zeolite as a catalyst produces in a single step benzene, toluene, xylene, and naphthalene, which can be used as building blocks by the petrochemical industry or further converted to gasoline-range hydrocarbons using hydrogenation processes already employed in refining.[8]

The isomorphous substitution of silicon with aluminum atoms in zeolites' well-defined crystal structure generates strong Brønsted acid sites, which can catalyze a broad range of cracking, isomerization, and alkylation reactions. The performance of a zeolite for a given reaction depends on its acid site density, pore size, and crystallographic structure (pore network dimensionality, presence of large cages).[9] ZSM-5 is particularly desirable for reactions involving small aromatics as its narrow pore size matches the dynamic diameter of benzene. Consequently, only molecules with similar size and shape can diffuse in or out of the crystal, making it an excellent catalyst for the production of benzene, toluene, para-xylene, and naphthalene.[8d]

ZSM-5-catalyzed fast pyrolysis of cellulose to aromatics has been investigated by numerous groups.[2, 8d, 9b, 10] Despite many efforts, commercial ZSM-5 samples from Zeolyst International offer amongst the highest reported yields of aromatic hydrocarbons to date and, therefore, these catalysts were employed in most of the recently published studies.[11] The reason for this better performance has not been identified yet and the lack of structure-activity correlations currently constitutes a major barrier for the rational design of ZSM-5 catalysts for CFP.

Several works attempted to further improve aromatics yield by enhancing diffusion and by passivating the ZSM-5's outer surface, two approaches commonly used in petrochemistry.[8d, 10a, 10c, 10e, 12] Zheng et al. hypothesized that the slow diffusion of reactants and products in the ZSM-5 micropores represents the main limiting factor to achieve a high performance.[10e] Therefore,

[a] T. C. Hoff, D. W. Gardner, Prof. J.-P. Tessonnier
Department of Chemical and Biological Engineering
Iowa State University
617 Bissell Road, 2138 Biorenewables Research Laboratory
Ames, IA 50011 (USA)
E-mail: tesso@iastate.edu
[b] R. Thilakaratne, Dr. K. Wang, Prof. R. C. Brown
Bioeconomy Institute
Iowa State University
617 Bissell Road, 1140E Biorenewables Research Laboratory
Ames, IA 50011 (USA)
[c] Dr. T. W. Hansen
Center for Electron Nanoscopy
Technical University of Denmark
Kgs. Lyngby, 2800 (Denmark)

Supporting information for this article is given via a link at the end of the document.

this team proposed to shorten the diffusion path by decreasing the size of the ZSM-5 crystals. The authors compared 2 µm, 200 nm, and 50 nm crystals. Unfortunately, the results were ambiguous as the 200 nm crystals showed the highest aromatic yield but the 50 nm ZSM-5 gave the highest yield of desired benzene, toluene, and xylene (BTX) products. Additionally, reaction residence times were 50 s, thus diminishing any benefits from improved diffusion. Modest improvements in overall aromatic yield were also observed after introducing mesopores in the zeolite crystals by desilication.[12b] Finally, passivation of the zeolite outer surface by silylation and dealumination was attempted in order to decrease the undesired conversion of pyrolysis vapors to coke on extra-framework aluminum sites.[10a] However, these post-synthetic modifications did not significantly impact the catalytic performance either.

Here, we synthesized and fully characterized series of ZSM-5 catalysts with different elemental composition, crystal size, porosity, and acidity in an effort to identify structure-property-activity relationships. Through the investigation of these samples and comparison with commercial ZSM-5 from Zeolyst and Clariant, we show that crystallinity and extra-framework aluminum, parameters neglected in previous studies, play a key role in catalyst performance. These findings prompted us to investigate alternative synthesis methods. A remarkable ZSM-5 catalyst that offered the highest aromatic hydrocarbon yield to date was obtained.

Results and Discussion

ZSM-5 with controlled particle size and mesoporosity was synthesized using a procedure developed by Petushkov et al.[13] This method produces ZSM-5 nanocrystals (primary particles) of 5.5 – 40 nm that self-organize into mesoporous aggregates (secondary particles) of approximately 200 nm. Mesopore surface area and volume can be tailored for these samples by varying the hydrothermal treatment temperature between 130 and 190 °C while keeping the gel composition constant.[13] The obtained zeolites were fully characterized in order to establish clear relationships between catalytic activity and catalyst properties, specifically crystallinity, elemental composition, porosity, and acidity.

Catalyst Characterization

SEM images (Fig. 1) revealed that the ZSM-5 samples synthesized at 130 – 190 °C were homogeneous and composed of nanocrystals organized in 200 – 600 nm aggregates, in good agreement with Petushkov et al.[13] The elemental composition of each sample was determined by X-ray energy dispersive spectroscopy (EDS) using an accelerating voltage of 15 kV. These conditions afforded a spatial resolution (analysis depth) of approximately 2 µm sufficient to obtain bulk chemical compositions for nanocrystalline samples. Measurements on commercial ZSM-5 of known chemical compositions confirmed that the SAR calculated from EDS analysis were accurate. The SAR values obtained for the laboratory synthesized nanocrystalline ZSM-5 samples ranged between 49 and 53 (Table 1). The only deviation was observed for the zeolite prepared at the lowest temperature (130 °C). Low temperature

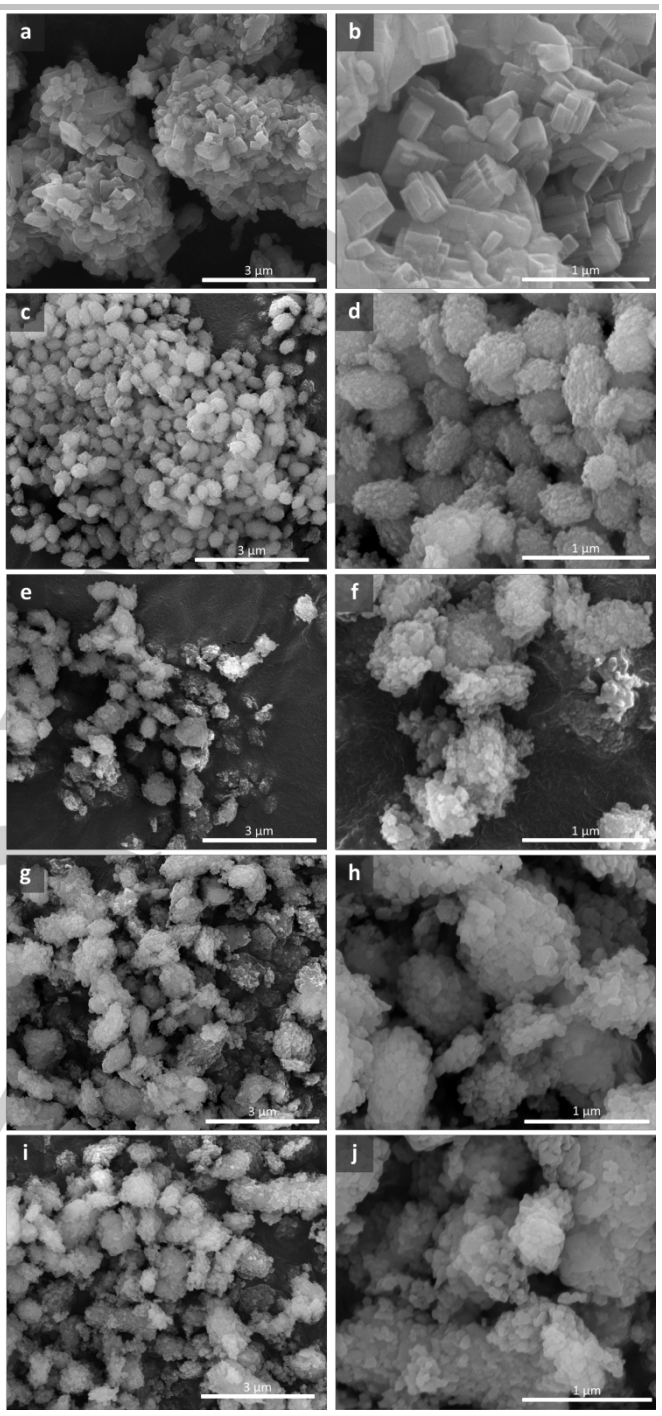

Figure 1. SEM images of commercial Zeolyst ZSM-5 CBV2314 (a,b) and hierarchical ZSM-5 samples synthesized at 130 °C (c,d), 150 °C (e,f), 170 °C (g,h), and 190 °C (I,j) for 24 h.

seemed to be detrimental to Al incorporation in the zeolite framework, which resulted in a SAR of 99.

Powder X-ray diffraction (XRD) patterns were acquired to study the samples' crystal structure and the presence of amorphous material (Fig. 2). An internal standard was mixed with each sample and used as a reference to calculate the relative crystallinity of the zeolitic material. Only diffraction peaks characteristic of the MFI framework type and internal standard

Table 1. Synthesis conditions and characterization data for commercial and laboratory synthesized ZSM-5 catalysts

Catalysts[a]	Synthesis		SAR[b]	Surface area (m^2g^{-1})[c]			Volume (cm^3g^{-1})[d]		RC[e] (%)	^{27}Al FWHM[f] (nm)	NH_3-TPD BAS Peak[g]	
	Time (h)	Temp (°C)		S_{total}	S_{micro}	S_{meso}	V_{total}	V_{micro}			Ctr. (°C)	Area (a.u.)
CBV2314	--	--	23	372	274	98	0.202	0.127	100.0	5.9	408	86
ZSM5-24-130	24	130	98.6	481	230	251	0.348	0.105	81.0	5.6	366	30
ZSM5-24-150	24	150	49.2	438	254	184	0.364	0.117	86.7	5.8	387	39
ZSM5-24-170	24	170	52.9	398	248	150	0.273	0.114	100.9	5.4	409	66
ZSM5-24-190	24	190	52.3	421	243	178	0.291	0.111	102.5	5.3	413	68
ZSM5-OPT	40	180	34.4	318	244	74	0.159	0.113	100.7	4.9	432	147

[a] CBV2314: commercial ZSM-5; ZSM5-24-xxx: nanocrystalline ZSM-5 synthesized with various hydrothermal treatment temperatures (xxx=130-190 °C) using the method by Petushkov et al.[13]; ZSM5-OPT: microcrystalline ZSM-5 synthesized using a recipe adapted from Kleinwort.[14] [b] Silica-to-alumina ratio calculated from EDS analysis. [c] Specific surface areas determined from N_2 physisorption using the BET (total) and t-plot (micropores) methods. The mesoporous surface area was calculated by difference. [d] Total and microporous volumes determined by N_2 physisorption using the single-point adsorption pore volume (total) and t-plot (micropores) methods. [e] Relative crystallinity calculated based on the intensity of the main diffraction peaks. Results were normalized to the commercial CBV2314. [f] Full width at half maximum (FWHM) of the ^{27}Al SSNMR peak corresponding to framework aluminum. [g] Peak center and area for the contribution corresponding to strong Brønsted acid sites in the NH_3-TPD curves.

were observed. In the present work, the relative crystallinity was calculated using the intensity of characteristic reflections instead of the diffraction peak areas. While both methods are common, the peak intensity is more sensitive to small variations in crystal structure. Temperature was found to have a beneficial effect on the crystallization process in good agreement with Petushkov et al.[13] The intensity of the reflections at 23.08, 23.88, and 24.36° increased by 27 % in going from a 130 to 190 °C synthesis temperature. A lower crystallinity was accompanied by an increase of the amorphous phase in the sample, as indicated by a more pronounced amorphous scattering halo. Small peak shifts of 2θ = + 0.1° were also observed for the least crystalline samples, e.g. ZSM5-24-130, representative of a small contraction of the framework (smaller d spacing).

Nanostructuring the catalyst increased the total surface area from 372 m^2/g to 377 – 480 m^2/g (Table 1). A greater surface-to-volume ratio for these small crystals and their arrangement in aggregates resulted in a 3-fold enhancement of the mesoporosity compared to that of the commercial zeolite (Table 1). This increase is evident in the N_2 physisorption isotherms at high P/P_0 and in the pore size distributions (PSD) (Fig. 3). While the commercial ZSM-5 gave a type IV isotherm with a narrow H4 hysteresis typical of microporous materials organized in disordered mesoporous aggregates, all synthesized samples showed a more pronounced hysteresis loop characteristic of hierarchical materials.[15] The pore size distributions (calculated from the adsorption branch of the isotherm using the BJH model) revealed a broad distribution of mesopores from 5 to 50 nm for samples synthesized at 130 – 150 °C whereas higher synthesis temperatures favored the formation of more compact aggregates. Pores upwards of 50 nm are significantly larger than those observed in MCM-41 or SBA-15 and, therefore, diffusion is expected to be significantly improved for the samples synthesized at 130 and 150 °C.

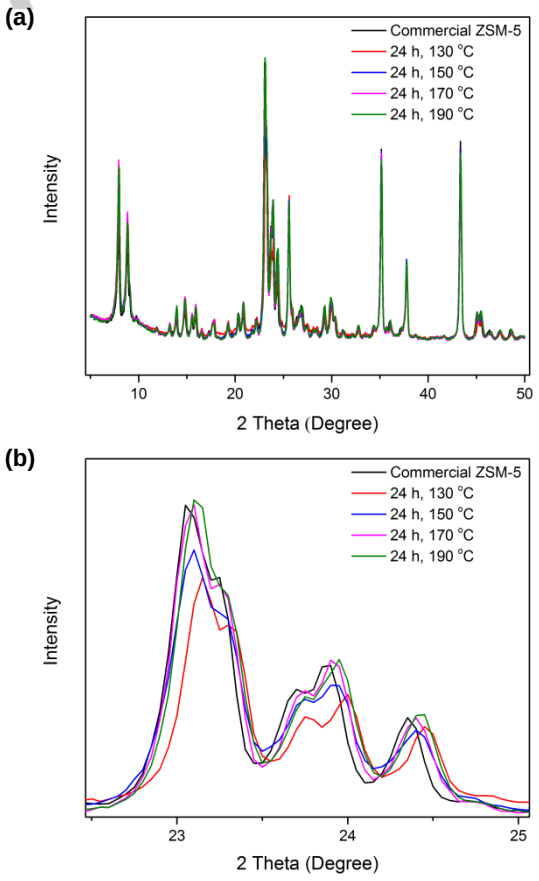

Figure 2. Powder XRD patterns obtained for commercial (CBV2314) and for nanocrystalline samples synthesized at various temperatures. (a) The addition of an internal standard allowed us to scale the patterns and compare characteristic MFI peaks (b).

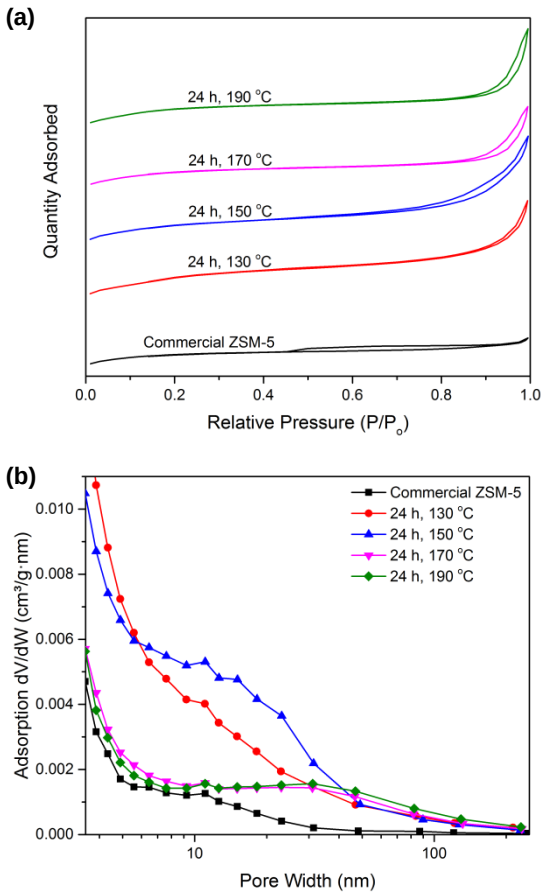

Figure 3. N_2 isotherms (a) and pore size distributions (b) of commercial (CBV2314) and synthesized hierarchical ZSM-5 samples.

Changes in acidity were probed by ammonia temperature programmed desorption (NH_3-TPD, Fig. 4) and Fourier transform infrared spectroscopy of pyridinated samples (Pyridine-FTIR, Fig. 5), two complementary techniques commonly used for zeolite characterization.[16] NH_3-TPD curves obtained for similar zeolites measured under the same conditions provides valuable information on changes in total (Lewis and Brønsted) acid site density within a sample series.[16] Figure 4 reveals a net increase in acidity with synthesis temperature, independent of elemental composition. These results suggest a better aluminum insertion in the zeolites. While it is difficult to distinguish Lewis from Brønsted acid sites by NH_3-TPD, Bates et al. demonstrated a direct correlation between the contribution at 366-413 °C and N-propylamine decomposition.[17] Therefore, this TPD peak can be unambiguously assigned to strong Brønsted acid sites associated to framework Al atoms. An integration of this contribution (Table 1) supports an increase in BAS with synthesis temperature, in good agreement with improved Al insertion in tetrahedral framework sites at the expense of amorphous Al species. This interpretation is also consistent with pyridine-FTIR and ^{27}Al solid state nuclear magnetic resonance (SSNMR) data (*vide infra*). It is also worth noting that the BAS peak center shifted from 366 to 413 °C with increasing synthesis temperature, which indicates the presence of stronger Brønsted acid sites in the more crystalline samples.

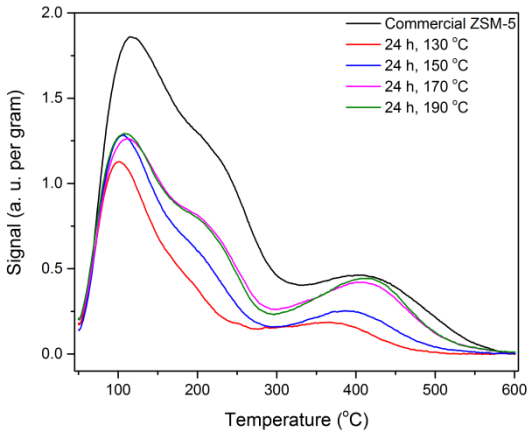

Figure 4. Ammonia temperature-programmed desorption (NH_3-TPD) curves obtained for commercial (CBV2314) and the synthesized samples.

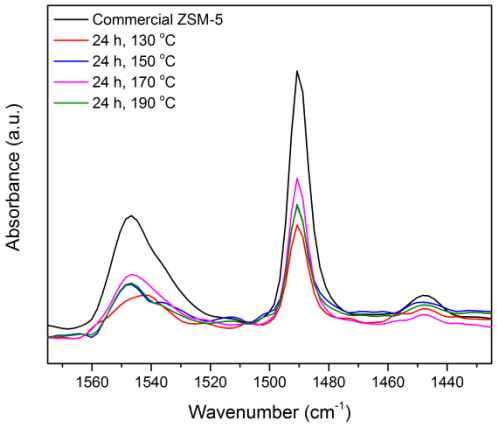

Figure 5. Fourier transform infrared (FTIR) spectra of pyridinated samples. The peaks at 1550 and 1455 cm^{-1} are characteristic of Brønsted and Lewis acid sites, respectively.

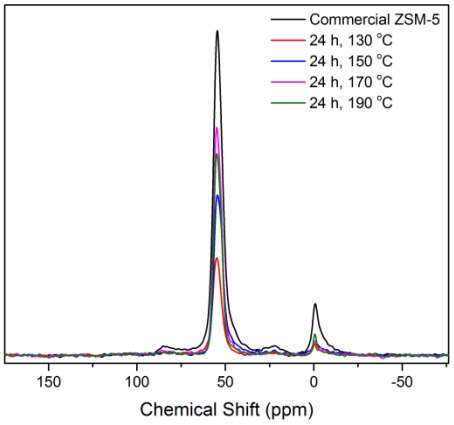

Figure 6. ^{27}Al solid state nuclear magnetic resonance (SSNMR) spectra of the commercial (CBV2314) and synthesized ZSM-5 samples. The peaks at 55 ppm and 0 ppm are characteristic of Al atoms in framework and extra-framework sites, respectively.

Changes in acidity were further investigated by Pyridine-FTIR as this probe molecule generates distinct IR-active vibrations when chemisorbed on Lewis and Brønsted acid sites (Fig. 5). Interestingly, integration of the peak at 1455 cm^{-1} revealed similar concentrations of Lewis acid sites, independent of the synthesis parameters. The concentration of Brønsted acid sites (~1550 cm^{-1}) increased according to 130<150<170≈190 °C. This trend is consistent with the changes observed in the ^{27}Al SSNMR spectra (Fig. 6 and S1-S2). The obtained SSNMR spectra displayed two main peaks centered at 55 ppm and 0 ppm, corresponding to tetrahedrally coordinated framework aluminum atoms (Al_{Td}) and octahedral extra-framework Al species (Al_{Oh}), respectively. The isomorphous substitution of framework silicon with aluminum in the tetrahedral coordination creates negative framework charges that are balanced by protons, giving zeolites their characteristic strong Brønsted acidity.[18] The linear correlation between Brønsted acid sites (H^+) and tetrahedrally coordinated Al atoms allows for the quantification of strong Brønsted sites in protonic zeolites by SSNMR.[17] In contrast to chemisorption techniques, SSNMR probes the total number of strong Brønsted acid sites (associated to framework Al), regardless of their accessibility. Therefore, the fact that SSNMR (Al_{Td} peak), NH_3-TPD, and Pyridine-FTIR share the same 130<150<170≈190 °C trend indicates that all the Brønsted acid sites are accessible and titrated in the equilibrated samples, when NH_3 and pyridine are given sufficient time to diffuse inside the pore network. At this stage, it is also important to remember that the samples synthesized at 130 and 150 °C present the highest mesopore surface area and volume (Table 1). Yet, these samples are the least acidic. These results indicate that our series of nanocrystalline ZSM-5 samples is fundamentally different from the zeolites studied by Puértolas et al.[19] These authors identified a clear porosity-acidity correlation for mesoporous zeolites prepared by desilication. Hence, porosity, acid site density, and catalytic activity followed the same trend. In contrast, all the techniques used in the present study indicate that the number of strong Brønsted acid sites increases with synthesis temperature while the amount of amorphous material in the samples decreases, as indicated by XRD. Therefore, higher synthesis temperatures (170-190 °C) enhances Al insertion in the zeolitic framework at the expense of Al atoms involved in amorphous, NMR-invisible, extra-framework material, with an optimum at 170 °C for the gel composition selected for this work.

The complex relationship between the characterized properties reveal why clear structure-activity correlations have not yet been identified for zeolite-catalyzed fast pyrolysis. The combination of techniques used in the present work is expected to provide unique insights into these correlations.

Catalytic Performance

The synthesized samples were tested for the catalytic fast pyrolysis (CFP) of cellulose to aromatic hydrocarbons. Yields and selectivities to the most important products are reported in Fig. 7. It should be noted that the CFP reaction is typically performed at high temperature, between 600 and 800 °C. The optimal temperature (the temperature which affords the highest yields) varies depending on the configuration of the pyrolyzer used for the tests. While pyroprobes are typically operated at 600-650 °C, micro-pyrolyzers perform better at 650-700 °C.[2b, 9b] Here, we chose to carry out the reaction at 700 °C in a micro-pyrolyzer based on previous optimizations of our setup.[2b] Cellulose and catalyst were brought to the target temperature within 500 ms and the overall reaction proceeded within a few seconds. Only aromatic hydrocarbons were detected under these conditions, with benzene, toluene, xylene, and naphthalene accounting for more than 70% of the detected products.

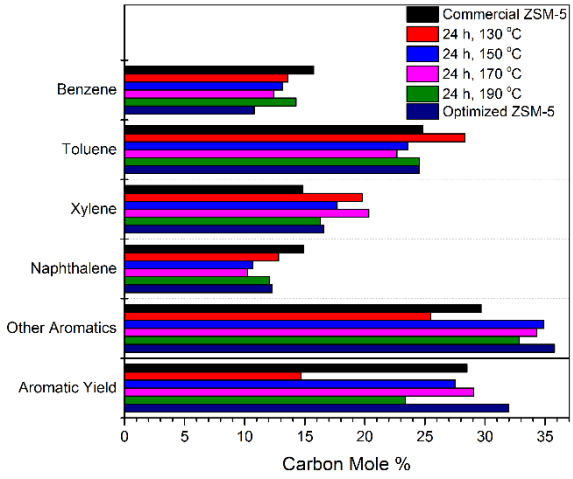

Figure 7. Aromatic yield and selectivity to the main aromatic hydrocarbons obtained for the catalytic fast pyrolysis of cellulose at 700 °C. The tests were performed using a micro-pyrolyzer equipped with online GC-MS analysis.

Significant differences in activity were observed for the nanocrystalline zeolites with yields to aromatic hydrocarbons ranging between 15 and 30%. This broad differences in catalytic performance cannot be attributed to variations in elemental composition as commercial ZSM-5 samples from Zeolyst and Clariant with SAR of 23 to 55 achieved similar yields under our reaction conditions (27.5 ± 1.0 %, see Table S1). Interestingly, the laboratory synthesized zeolites with the highest mesoporosity (ZSM5-24-130 and ZSM5-24-150) performed very differently and gave yields of 15 and 27%. These results are important: while mesoporosity and small crystal size may enhance intracrystalline diffusion,[9a] other parameters play a more prominent role on the production of aromatic hydrocarbons. This interpretation is consistent with previous work for which only minor improvements in BTX production were achieved when introducing mesopores in zeolite crystals.[12b]

Comparing the reference CBV2314 with the hierarchical ZSM-5 synthesized at 150, 170, and 190 °C provided interesting insights into the parameters that govern the catalytic activity. These 4 zeolites achieved similar yields (24-29%) although they exhibit very different crystal size, aggregate size, porosity, and acidity. It is also worth noting that ZSM5-24-170 achieved the same yield as the commercial ZSM-5 (CBV2314) despite having 25% fewer BAS and a lower microporous volume, which were

both reported to be critical to achieve a high aromatic hydrocarbon yield for the CFP of cellulose.[10a, 10e]

Key features and aromatic yields for the least active (ZSM-24-130) and the best catalysts (ZSM5-24-170 and CBV2314) were compared in a radar plot in order to visually identify key differences and guide future rational catalyst design (Fig. 8). The overlapping areas in the plot reveal that the best catalysts are highly crystalline and present a strong acidity. These observations were consistent for commercial Zeolyst and Clariant zeolites (Table S2, Fig. S3) as well as laboratory synthesized ZSM-5. More surprisingly, mesoporosity (S_{meso}) and total surface area (S_{total}) do not seem to play a significant role on aromatic hydrocarbon production under our reaction conditions. New correlations also emerged between catalytic activity and Al_{Td} NMR peak intensity and shape. Correlations between Al_{Td} peak intensity, acidity, and catalytic activity were identified and have already been discussed in previous sections. However, these correlations failed to explain why ZSM5-24-170 achieved the same aromatic yield as commercial ZSM-5 with 50% fewer acid sites. More in depth analysis of the SSNMR results revealed interesting trends in the shoulder at ~50 ppm (Fig. S1) and in the full width at half maximum of the Al_{Td} peak (Table 1). These observations could be consistent with the presence of extra-framework amorphous silica-alumina in the commercial zeolite as well as in the ZSM5-24-130 and ZSM5-24-150 samples (also revealed by XRD).[20] Therefore, as a next step, we explored alternative gel compositions and hydrothermal treatment conditions that favor the growth of highly crystalline ZSM-5 samples with strong acidity and enhanced Al insertion in the zeolitic framework as these parameters seem critical to achieve high yields (*vide infra*).

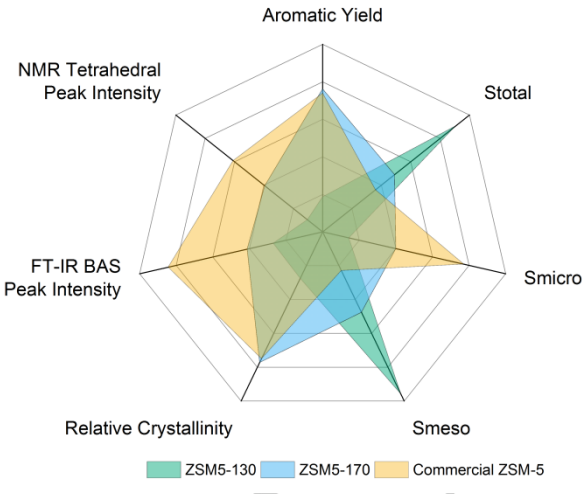

Figure 8. Radar plot highlighting key structural and chemical features of commercial ZSM-5 CBV2314 and hierarchical ZSM-5 synthesized at 130 and 170 °C.

Synthesis of ZSM-5 with Enhanced CFP Performance

The negligible amount of amorphous materials identifiable by XRD in samples synthesized at high temperature suggests a significant increase in bulk crystallinity would be difficult to achieve. However, disordered surface species (*e.g.* amorphous extra-framework silica-alumina) have been proposed to block a vast majority (>99 %) of pore openings in small (<50 nm) MFI

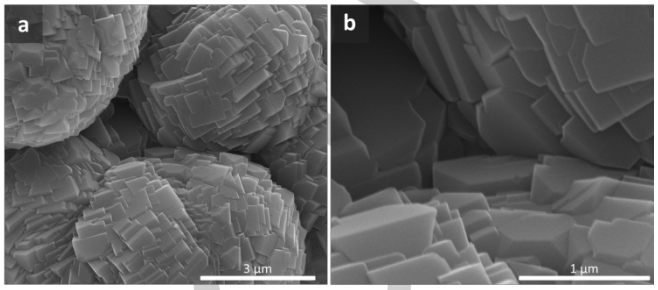

Figure 9. Low (a) and high (b) magnification SEM images of the optimized ZSM-5 sample.

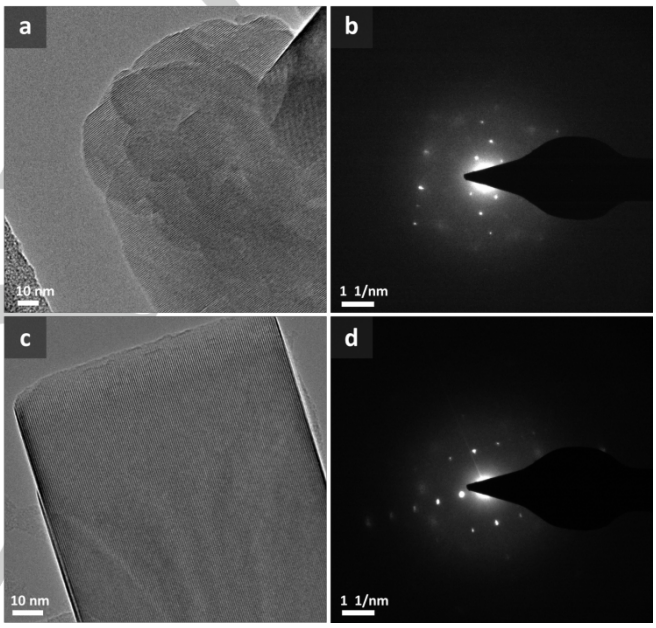

Figure 10. Aberration-corrected HRTEM images of commercial CBV2314 (a) and the optimized ZSM-5 sample (b). The corresponding selected area electron diffraction (SAED) patterns (respectively c and d) reveal a lower amount of amorphous species in the optimized zeolite.

crystals.[21] These blockages are particularly difficult to characterize by aberration-corrected high-resolution transmission electron microscopy (AC-HRTEM), atomic force microscopy (AFM), and even chemisorption.[21] While most acid sites remain accessible to probe molecules under equilibrium conditions, frequency response investigations demonstrated that these inorganic species hamper the diffusion of bulky molecules under reaction conditions. Obviously, these effects are expected to also take place for larger crystals, in particular for very fast reactions such as CFP. We hypothesized that tuning the synthesis conditions to lower the formation of these disordered species would also improve Al insertion into the zeolitic framework and enhance the catalytic activity.

Highly ordered (defect free) zeolites are of particular importance for membrane applications where inter-crystal

diffusion paths and varying pore sizes are detrimental to membrane performance.[22] Research in this field has established that heterogeneous nucleation growth techniques and extended crystal growth times are advantageous for single-phase MFI synthesis.[22] Through these synthesis techniques, we can minimize defect formation and generate highly ordered crystals at the expense of mesoporosity.

The synthesis of a highly ordered ZSM-5 catalyst was adapted from a recipe by Kleinwort.[14] The method utilizes a seeding step and long crystallization time to ensure a highly homogeneous and crystalline ZSM-5. SEM images of the obtained sample revealed microcrystals organized in aggregates of 3-5 µm, i.e. approximately one order of magnitude larger than the nanocrystals studied in the first part of this work (Fig. 9). Characterization by XRD (Fig. S4) confirmed that the sample's crystallinity was similar to commercial ZSM-5 (RC=100.7%). However, AC-HRTEM and selected area electron diffraction (SAED) showed differences in the structure and amorphous content for the two samples (Fig. 10 and S5-S6). Small (20-50 nm) crystalline domains with a significant number of grain boundaries and low contrast areas which could correspond to amorphous regions were imaged for the commercial Zeolyst CBV2314. The corresponding SAED pattern was found to be consistent as it showed the coexistence of highly crystalline (bright spots) and amorphous (diffuse spots) regions. In contrast, the optimized ZSM-5 crystals have a well-aligned network of micropores extending over hundreds of nanometers. The sample's high crystallinity was further confirmed by SAED.

As expected, the mesoporous surface area and volume were minimal (sample ZSM5-OPT in Table 1). N_2 physisorption showed a near-type I isotherm characteristic of microporous materials and the pore size distribution displayed only few pores with a width greater than 1 nm (Fig. S7-S8). Hence, while the relative crystallinity determined by XRD is similar for both samples, the optimized ZSM-5 exhibits long-range order with micropores free of any amorphous material.

The existence of pore blockages in both samples was further studied by nitrogen uptake kinetic studies (Fig. 11). These time-resolved nitrogen adsorption experiments provide significant insights into the diffusion of small molecules with dynamic diameters well below the zeolite's pore size. The uptake experiments start after evacuating the samples and reaching a base pressure of 10 µmHg. Thus, the uptake kinetic traces provide direct information on the accessibility (and blockage) of the zeolite's microporous network. Figure 11 clearly shows that diffusion in the commercial ZSM-5 is slow and the adsorbed volume plateaued after ca. 50 s. In comparison, the uptake for the optimized ZSM-5 was about one order of magnitude faster despite the larger crystal and aggregate sizes (Fig. 9). These experiments, together with AC-HRTEM images and SAED patterns, support the presence of an amorphous phase inside the pores of the commercial zeolite and that may impact its catalytic activity.

Optimized ZSM-5 catalyzed fast pyrolysis of cellulose produced 32% yield of aromatic hydrocarbons, a 12% increase compared to commercial CBV2314 tested under the same conditions (Fig. 7). To the best of our knowledge, this is the first time that the performance of Zeolyst ZSM-5 has been surpassed. It is worth noting that this excellent performance was obtained with microporous micron-sized crystals. Therefore, this experiment is consistent with the conclusions drawn from the first part of this work and confirms that while nanostructuring the zeolite crystals or inserting mesopores and mesovoids may help

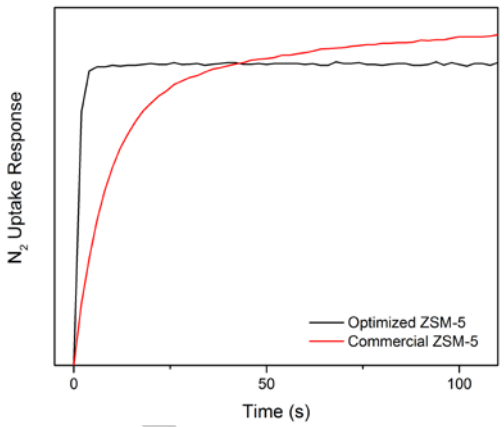

Figure 11. N_2 uptake curves for commercial and optimized ZSM-5.

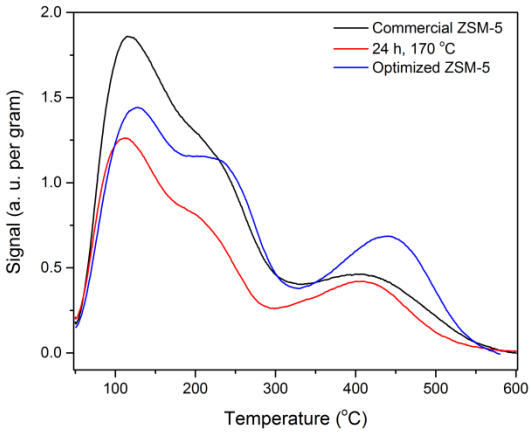

Figure 12. NH_3-TPD curve obtained for optimized ZSM-5. The curves corresponding to commercial ZSM-5 and to the hierarchical ZSM5-24-170 sample are also shown for comparison. The optimized sample exhibits a more pronounced high temperature desorption peak despite a lower Al content compared to commercial CBV2314. The peak is also shifted to higher temperature, which is an indication for stronger acidity.

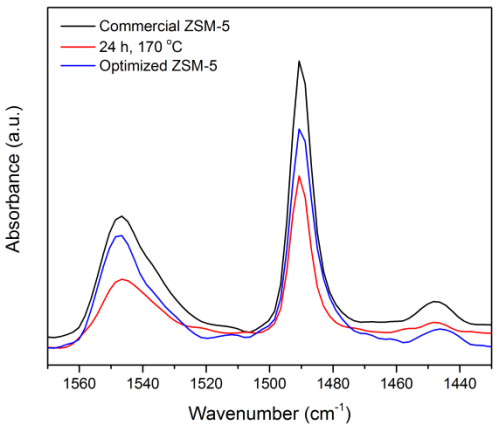

Figure 13. FTIR spectra of pyridinated samples. Compared to the commercial zeolite used here as a reference, the optimized ZSM-5 exhibits only slightly lower Brønsted acidity despite a 50% lower Al content by EDS analysis.

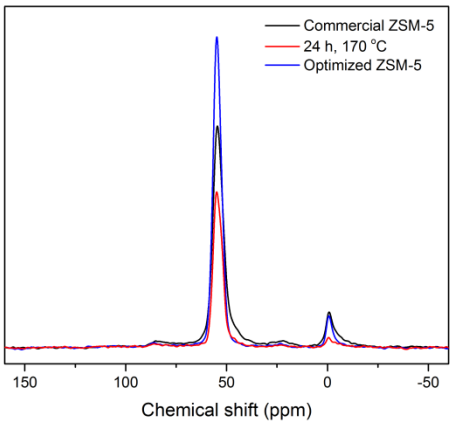

Figure 14. ^{27}Al SSNMR spectrum of optimized ZSM-5. The spectra for commercial ZSM-5 and ZSM5-25-170 are displayed for comparison.

inter- and intracrystalline diffusion, other parameters have a significantly more pronounced impact on the CFP activity and the formation of the desired aromatic hydrocarbons.

Further analysis of the microcrystalline ZSM-5 by NH_3-TPD, pyridine-FTIR, and ^{27}Al SSNMR (Figs. 12-14) confirmed that the synthesis conditions we used to minimize defects also enabled a better insertion of Al in the zeolitic framework and, as a result, the formation of more homogeneous and stronger Brønsted acid sites. While the sample presents a SAR of 34.4, thus a 50 % lower Al content than that of the commercial ZSM-5, NH_3-TPD revealed a significant increase in strong acid sites (Fig. 12). Conversely, pyridine-FTIR displayed a similar increase, although less pronounced (Fig. 13). This apparent discrepancy is most likely due to CBV2314 exhibiting weak acid sites that are captured by Pyridine-FTIR but not by NH_3-TPD due to the easy desorption of ammonia. Extra-framework AlOH groups are strong enough to retain pyridine at the desorption temperature used for pyridine FTIR. However, the NH_3 desorption activation energy for AlOH sites is lower than for Brønsted acid sites.[23] Therefore, AlOH would not appear in the strongest acid site region of TPD (above 350 °C). Further FTIR studies using collidine and 2,6-di-*tert*-butylpyridine (DTBPy), two probe molecules too large to diffuse inside the ZSM-5 micropore network, were performed in order to locate these AlOH sites and get additional information on acid site accessibility.[24] The absence of any signal for this sample series (Fig. S9) demonstrate that the extra-framework AlOH species are located inside the pore network, in good agreement with the N_2 uptake experiments. These measurements also unambiguously ruled out any significant contribution from external acid sites and any porosity-acidity correlation for CFP. This interpretation is also supported by ^{27}Al SSNMR results (Fig. 14): the peak corresponding to tetrahedral aluminum increases in intensity and becomes narrower, indicating more Al in highly symmetric framework sites than for the commercial sample. Using the radar plot in Fig. 15, we again highlight the critical parameters for high catalytic activity and provide further insight into key factors that need to be further optimized. Comparing the results for commercial and optimized ZSM-5 reveals that the increase in aromatic hydrocarbon yield can be assigned to a higher Al ratio in framework sites and, reciprocally, less Al in extra-framework surface species that block pores and, potentially, catalyzed undesired reactions.

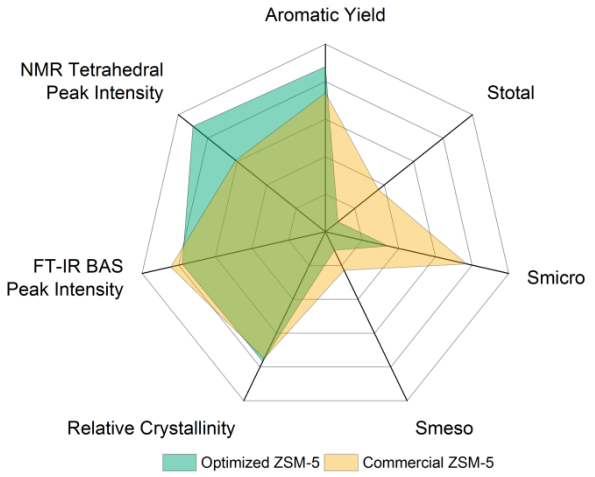

Figure 15. Radar plot highlighting key structural and chemical features of commercial ZSM-5 and the optimized zeolite obtained in this work through combination of seeded growth and extended crystallization times.

Conclusions

The ZSM-5 zeolite catalyzes the fast pyrolysis of cellulose with a high selectivity to small aromatic hydrocarbons (benzene, toluene, xylene, naphthalene), which find applications as bio-based chemicals or as gasoline-range fuels after additional hydrogenation. The unique size and shape selectivity of ZSM-5 towards these compounds is well-established and understood. However, the importance of other structural parameters for the efficient transformation of pyrolysis vapors into aromatics remained to be elucidated. It was previously proposed that strong Brønsted acid sites located inside the pores of the zeolite catalyze a series of deoxygenation, cracking, alkylation, and aromatization reactions. This hypothesis was primarily based on analogies with the methanol to olefins (MTO) and methanol to hydrocarbons (MTH) reactions. Here, we have demonstrated that amorphous silica-alumina surface species, even present in small concentration, impact the diffusion of bulky reactants, lower the amount of Al in framework sites and, consequently, alter the Brønsted acid site density and strength. These observations were shown to hold without exception regardless on the provider or synthesis method. Based on this finding, we designed a highly crystalline zeolite with minimal crystalline defects and amorphous material through the adaptation of techniques developed for zeolite membrane synthesis. This approach allowed us to further study the role of zeolite crystallinity, as well as the nature of its acid sites. The yield to desired products increased by 12% and for the first time surpassed the aromatic hydrocarbon yield obtained for commercial ZSM-5 tested under the same conditions. This

work sets the foundation for future mechanistic studies and for the design of new zeolitic materials optimized for CFP.

Experimental Section

Catalyst Synthesis

Reference ZSM-5 samples in their ammonium form were purchased from Zeolyst International and used here for comparison: CBV2314, CBV3024E, CBV5524G, and CBV8014 with SiO_2/Al_2O_3 = 23, 30, 50, and 80, respectively. The samples were calcined in air at 550 °C for 10 h (ramp: 5 °C/min) before characterization and catalytic testing. ZSM-5 nanocrystals with controlled particle size and mesoporosity were synthesized using the procedure previously published by Petushkov et al.[13] In short, a clear gel with the following molar composition was prepared: 25 TEOS : 1 $NaAlO_2$: 5 TPAOH : 4 TPABr : 1000 H_2O, where TPAOH = tetra-*n*-propylammonium hydroxide (Alfa Aesar, 40%), TPABr = tetra-*n*-propylammonium bromide (Sigma-Aldrich, 98%), and TEOS = tetraethyl orthosilicate (Aldrich, 98%). One third of the water, TPAOH, and sodium aluminate (Strem Chemicals, 99.9%) were mixed together and stirred at 500 RPM for 5 min to ensure the complete dissolution of the aluminate. The remaining water and TPABr were then added and the mixture was stirred for an additional 5 min at 500 RPM. Finally, TEOS was mixed into the solution and stirred overnight at room temperature in a closed polypropylene flask. The resulting clear gel was loaded into a Teflon lined Paar stainless steel autoclave (Parr 4744) and placed in the middle of a pre-heated mechanical convection oven (ThermoScientific Heratherm OMS100) for 24 h. The synthesis temperature was varied from 130 to 190 °C. Following synthesis, zeolite crystals were collected by centrifugation (5,000 RPM, 30 min) and washed twice with DI water and once with ethanol. After the final washing, the slurry was dried at 70 °C overnight. The sample was then calcined at 550 °C for 10 h (ramp: 5 °C/min) to decompose the TPA structure directing agent. Finally, the acid form of the ZSM-5 was obtained after 3 successive ion exchanges with a 0.5 M NH_4NO_3 (Fisher Scientific, ACS) solution at 70 °C, drying at 70 °C for overnight, and calcination at 550 °C for 10 h. The optimized zeolite was synthesized according to the following procedure adapted from Kleinwort.[14] Seeding gel was prepared by adding 0.69 g Sodium Hydroxide and 5.85 g 20 wt% TPAOH to 35.51 g DI water and stirring at 500 rpm for 5 minutes. Silicic acid (7.945 g) was slowly added under stirring and the solution further stirred for one hour at 500 rpm. The seeding gel was then aged at 100 °C for 16 hours. Synthesis gel was prepared by mixing 86.78 g DI water, 0.88 g sodium hydroxide, and 1.03 g Sodium Aluminate. The solution was stirred at 500 rpm for 5 min. Silicic acid (11.31 g) was slowly added under stirring and the mixture was stirred for one hour at 500 rpm. Seeding gel (5 g) was added to the synthesis solution and stirred for one hour at 500 rpm. The final synthesis gel was placed in stainless steel Teflon-lined autoclaves and crystallisation occurred at 180 °C for 40 hours. Following synthesis, samples were separated by centrifugation (5000 rpm for 15 minutes) and washed twice with DI water and once with ethanol. The zeolite was then dried at 105 °C for 24 hours. Calcination and ion exchange procedures were followed according to those used for the nanocrystalline samples.

Catalyst Characterization

Powder X-ray diffraction patterns were collected on a Siemens D 500 diffractometer using Cu Kα radiation, a diffracted-beam monochromator (graphite), and a scintillation detector. Data were recorded in the 2θ range 5 – 50° using a step size of 0.05° and a dwell time of 3 s per step. The instrument broadening of the diffraction system was determined using the NIST LaB_6 standard. All data was analysed using Jade software version 9.5. Test specimens were prepared by mixing the bulk sample with an internal standard (high purity corundum, Alpha Aesar, verified using NIST 674b standards zincite, rutile and cerianite). The mixture consisted of 0.150 g of sample and 0.100 g of corundum. All measurements were made using an analytical balance and recorded to the nearest 0.1 mg. Then the components were mixed in an agate mortar-and-pestle. After mixing, the material was removed from the mortar, quickly recombined, and then placed back into the mortar-and-pestle for a second mixing cycle. This produced a homogeneous powder that contained 40% internal standard by mass. Specimens for XRD analysis were prepared by placing 0.20 ± 0.03 g of powder into the cavity of a zero-background holder (MTI Corporation zero diffraction plate, size 20 mm diameter by 1 mm deep). The powder was compacted into the cavity using a glass slide. Relative crystallinity was calculated by summing the peak maximums for each sample at the characteristic peaks 2Θ = ~23.08, 23.88, and 24.36°. Intensities are reported relative to the commercial sample (CBV2314) which was taken as 100%.

N_2 adsorption/desorption isotherms and N_2 uptake were measured with a Micromeritics ASAP 2020 system at 77 K. Zeolite powder (50 – 60 mg) was degassed at 200 °C (heating ramp: 5 °C/min) for 12 h under vacuum. The specific surface area was calculated using the Brunauer-Emmett-Teller (BET) method. The Barret-Joyner-Halenda (BJH) model with Faas correction was applied to the adsorption branch of the isotherm to calculate the pore size distribution. The *t*-plot method was used to discriminate between micro- and mesoporosity. N_2 rate of adsorption experiments were performed by dosing 5 cm^3/g of N_2 to a sample under vacuum (10 µmHg).

Scanning electron microscopy (SEM) images were acquired with a FEI Quanta 250 FEG operated at 10 kV. The samples were coated with 2 nm of iridium for conductivity. X-ray analysis was done with an Oxford Instruments Aztec™ energy-dispersive spectrometer (EDS) system equipped with an X-Max 80 detector. EDS spectra were typically recorded at 15 kV, corresponding to a beam penetration depth of about 2 µm.

For HRTEM and SAED, the samples were dry-dispersed on a holey carbon grid. Images and diffraction patterns were acquired on an FEI Titan 80-300 equipped with an aberration corrector on the objective lens. The microscope was operated at an acceleration voltage of 300kV. In order to minimize the effect of the electron beam, a low current density was used.

NH_3 temperature-programmed desorption (NH_3-TPD) was performed with a Micromeritics Autochem II 2920. Zeolite powder (50 mg) was pre-treated at 600 °C (heating ramp: 10 °C/min) in 10 ml/min He for 3 h to desorb any moisture from the surface. The sample was then cooled to 50 °C and ammonia was adsorbed for 30 min (20 ml/min of 10 vol% NH_3 in He). The sample was then purged at 100 °C under flowing He for 90 min. NH_3 desorption was recorded by heating the zeolite from 100 to 700 °C using a 10 °C/min ramp. Curves were normalized using the sample mass. Peak areas were determined using a Gauss analysis in OriginPro 9.1 software.

Characterization by Fourier transform infrared spectroscopy (FTIR) was performed on a Bruker Vertex 80 spectrometer with a Harrick Praying Mantis diffuse reflection (DRIFTS) attachment. Samples were first pyridinated or adsorbed with 2,6-di-tert-butylpyridine (DTBPy) for 48 h. Desorption occurred at 150 °C over 4 hours for pyridine and 1 h for DTBPy to remove any physisorbed species. A 2% pyridinated zeolite / KBr mixture was made, mixed and ground by mortar and pestle, and sieved with a 45 µm sieve. DTBPy samples were ground by mortar and pestle and sieved with a 45 µm sieve. The samples were then analyzed using OPUS 7.0 software. Absorbance from 4000 – 1000 cm^{-1} was collected using 32 scans at a 4 cm^{-1} resolution for pyridine and 128 scans at 2 cm^{-1} resolution for DTBPy.

The solid state nuclear magnetic resonance (SSNMR) measurements were performed on a Bruker Avance II spectrometer with a 14.1 T wide-bore magnet using a 4 mm triple resonance magic angle spinning (MAS) probe in double resonance mode. Topspin 3.0 software was used for data acquisition and processing. The operating frequencies for ^{1}H and ^{27}Al on this spectrometer are 600.13MHz and 156.38 MHz, respectively. The samples were first re-hydrated in a humidifier for 48 h at ambient temperature. The powders were then packed into a kel-F rotor insert and the insert was placed in a 4 mm MAS rotor. Samples were spun at a frequency of 5 or 12 Khz, with the slower speed required for some samples when spinning sidebands from the downfield peak interfered with the resonance of the upfield peak. The temperature was stabilized at 298K. Spectra were acquired using a 90-t-180–t–detect Hahn echo pulse sequence with a 2.5 µs 90° ^{27}Al pulse and an echo period of one rotor period (200 µs at 5 kHz spinning speed or 83 µs at 12 kHz spinning), under ^{1}H dipolar decoupling at 62 kHz. Spectra were typically acquired with 2048 scans and a recycle delay of 1.5 s.

Catalyst Testing

Catalytic pyrolysis experiments were conducted in a micro-pyrolyzer (PY-2020iS, Frontier Laboratories, Japan) equipped with an auto-shot sampler (AS-1020E, Frontier Laboratories, Japan). The detailed description of the setup can be found in previous studies.[2b, 25] All catalytic fast pyrolysis experiments were performed in-situ. The zeolite catalyst was mixed directly with biomass in a catalyst-to-biomass weight ratio of 20. Approximately 5 mg of biomass/catalyst mixture were used in a typical experiment. Helium carrier gas was used to sweep the pyrolysis vapour into the GC (Varian CP3800, USA). The vapour was separated in a GC capillary UA-1701 column. The GC oven was programmed for a 3-minute hold at 40 °C followed by heating (10 °C/min) to 250 °C, after which temperature was held constant for 6 minutes. The injector temperature was 260 °C and the injector split ratio was set to 100:1. Separated pyrolysis vapours were analysed either by a mass spectrometer detector (MSD) or a flame ionization detector (FID). The MSD (Saturn 2200, Varian, USA) was used for molecular identification. After the peaks were identified, standards were prepared to quantify the results using FID. The final product distribution was reported as molar carbon yield, defined as the molar ratio of carbon in a specific product to the carbon in the feedstock. Selectivity for aromatics in this study was defined as moles of carbon in a specific aromatic hydrocarbon to total moles of carbon in the aromatic products.

Acknowledgements

This work was supported by the Iowa Energy Center under IEC Grant Number 13-01. The authors would like to also thank Warren Straszheim and Scott Schlorholtz for their assistance with SEM and XRD investigations.

Keywords: heterogeneous catalysis • aluminum • zeolites • biomass conversion • pyrolysis

[1] a) M. S. Mettler, D. G. Vlachos, P. J. Dauenhauer, *Energy Environ. Sci.* **2012**, *5*, 7797-7809; b) G. W. Huber, S. Iborra, A. Corma, *Chem. Rev.* **2006**, *106*, 4044-4098; c) R. C. Brown, *Thermochemical Processing of Biomass: Conversion into Fuels, Chemicals and Power*, John Wiley & Sons, Chichester, **2011**; d) R. French, S. Czernik, *Fuel Process. Technol.* **2010**, *91*, 25-32.

[2] a) K. Wang, J. Zhang, B. H. Shanks, R. C. Brown, *Green Chem.* **2015**, *17*, 557-564; b) K. Wang, K. H. Kim, R. C. Brown, *Green Chem.* **2014**, *16*, 727-735.

[3] a) P. R. Patwardhan, J. A. Satrio, R. C. Brown, B. H. Shanks, *J. Anal. Appl. Pyrolysis* **2009**, *86*, 323-330; b) J. Zhang, M. W. Nolte, B. H. Shanks, *ACS Sustainable Chem. Eng.* **2014**, *2*, 2820-2830; c) M. S. Mettler, S. H. Mushrif, A. D. Paulsen, A. D. Javadekar, D. G. Vlachos, P. J. Dauenhauer, *Energy Environ. Sci.* **2012**, *5*, 5414-5424; d) A. D. Paulsen, M. S. Mettler, P. J. Dauenhauer, *Energy Fuels* **2013**, *27*, 2126-2134.

[4] a) H. Wang, J. Male, Y. Wang, *ACS Catal.* **2013**, *3*, 1047-1070; b) M. Stöcker, *Angew. Chem. Int. Ed.* **2008**, *47*, 9200-9211; c) J. Q. Bond, A. A. Upadhye, H. Olcay, G. A. Tompsett, J. Jae, R. Xing, D. M. Alonso, D. Wang, T. Zhang, R. Kumar, A. Foster, S. M. Sen, C. T. Maravelias, R. Malina, S. R. H. Barrett, R. Lobo, C. E. Wyman, J. A. Dumesic, G. W. Huber, *Energy Environ. Sci.* **2014**, *7*, 1500-1523; d) Y.-C. Lin, G. W. Huber, *Energy Environ. Sci.* **2009**, *2*, 68-80.

[5] D. Mohan, C. U. Pittman, P. H. Steele, *Energy Fuels* **2006**, *20*, 848-889.

[6] R. J. French, J. Hrdlicka, R. Baldwin, *Environ. Prog. Sustainable Energy* **2010**, *29*, 142-150.

[7] a) E. Furimsky, *Catal. Today* **2013**, *217*, 13-56; b) M. S. Talmadge, R. M. Baldwin, M. J. Biddy, R. L. McCormick, G. T. Beckham, G. A. Ferguson, S. Czernik, K. A. Magrini-Bair, T. D. Foust, P. D. Metelski, C. Hetrick, M. R. Nimlos, *Green Chem.* **2014**, *16*, 407-453; c) A. H. Zacher, M. V. Olarte, D. M. Santosa, D. C. Elliott, S. B. Jones, *Green Chem.* **2014**, *16*, 491-515.

[8] a) D. Kubička, I. Kubičková, J. Čejka, *Catalysis Reviews* **2013**, *55*, 1-78; b) E. Taarning, C. M. Osmundsen, X. Yang, B. Voss, S. I. Andersen, C. H. Christensen, *Energy Environ. Sci.* **2011**, *4*, 793-804; c) T. R. Carlson, T. P. Vispute, G. W. Huber, *ChemSusChem* **2008**, *1*, 397-400; d) J. Jae, G. A. Tompsett, A. J. Foster, K. D. Hammond, S. M. Auerbach, R. F. Lobo, G. W. Huber, *J. Catal.* **2011**, *279*, 257-268.

[9] a) J. Perez-Ramirez, C. H. Christensen, K. Egeblad, C. H. Christensen, J. C. Groen, *Chem. Soc. Rev.* **2008**, *37*, 2530-2542; b) T. R. Carlson, G. A. Tompsett, W. C. Conner, G. W. Huber, *Top. Catal.* **2009**, *52*, 241-252; c) Y. He, T. C. Hoff, L. Emdadi, Y. Q. Wu, J. Bouraima, D. X. Liu, *Catal. Sci. Technol.* **2014**, *4*, 3064-3073; d) L. Emdadi, Y. Wu, G. Zhu, C.-C. Chang, W. Fan, T. Pham, R. F. Lobo, D. Liu, *Chem. Mater.* **2014**, *26*, 1345-1355.

[10] a) A. J. Foster, J. Jae, Y.-T. Cheng, G. W. Huber, R. F. Lobo, *Appl. Catal., A* **2012**, *423–424*, 154-161; b) J. E. Robert, M. Thomas, in *Pyrolysis Oils from Biomass, Vol. 376*, American Chemical Society, **1988**, pp. 311-327; c) D. J. Mihalcik, C. A. Mullen, A. A. Boateng, *J. Anal. Appl. Pyrolysis* **2011**, *92*, 224-232; d) S. Shao, H. Zhang, L. Heng, M. Luo, R. Xiao, D. Shen, *Ind. Eng. Chem. Res.* **2014**, *53*, 15871-15878; e) A. Zheng, Z. Zhao, S. Chang, Z. Huang, H. Wu, X. Wang, F. He, H. Li, *J. Mol. Catal. A: Chem.* **2014**, *383–384*, 23-30.

[11] a) S. Wan, C. Waters, A. Stevens, A. Gumidyala, R. Jentoft, L. Lobban, D. Resasco, R. Mallinson, S. Crossley, *ChemSusChem* **2015**, *8*, 552-559; b) D. Santhanaraj, M. R. Rover, D. E. Resasco, R. C. Brown, S. Crossley, *ChemSusChem* **2014**, *7*, 3132-3137; c) T. R. Carlson, Y.-T. Cheng, J. Jae, G. W. Huber, *Energy Environ. Sci.* **2011**, *4*, 145-161.

[12] a) S. Kelkar, C. M. Saffron, Z. Li, S.-S. Kim, T. J. Pinnavaia, D. J. Miller, R. Kriegel, *Green Chem.* **2014**, *16*, 803-812; b) J. Li, X. Li, G. Zhou, W. Wang, C. Wang, S. Komarneni, Y. Wang, *Appl. Catal., A* **2014**, *470*, 115-122.

[13] A. Petushkov, S. Yoon, S. C. Larsen, *Microporous Mesoporous Mater.* **2011**, *137*, 92-100.

[14] R. Kleinwort, University of Hamburg **1995**.

[15] K. S. W. Sing, D. H. Everett, R. A. W. Haul, L. Moscou, R. A. Pierotti, J. Rouquérol, T. Siemieniewska, *Pure Appl. Chem.* **1985**, *57*, 603-619.

[16] N.-Y. Topsøe, K. Pedersen, E. G. Derouane, *J. Catal.* **1981**, *70*, 41-52.

[17] S. A. Bates, W. N. Delgass, F. H. Ribeiro, J. T. Miller, R. Gounder, *J. Catal.* **2014**, *312*, 26-36.

[18] D. Coster, A. L. Blumenfeld, J. J. Fripiat, *The Journal of Physical Chemistry* **1994**, *98*, 6201-6211.

[19] B. Puértolas, A. Veses, M. S. Callén, S. Mitchell, T. García, J. Pérez-Ramírez, *ChemSusChem* **2015**, *8*, 3283-3293.

[20] G. Crépeau, V. Montouillout, A. Vimont, L. Mariey, T. Cseri, F. Maugé, *The Journal of Physical Chemistry B* **2006**, *110*, 15172-15185.

[21] A. R. Teixeira, X. Qi, W. C. Conner, T. J. Mountziaris, W. Fan, P. J. Dauenhauer, *Chem. Mater.* **2015**, *27*, 4650-4660.

[22] M. C. Lovallo, M. Tsapatsis, *AIChE J.* **1996**, *42*, 3020-3029.

[23] F. Jin, Y. Li, *Catal. Today* **2009**, *145*, 101-107.

[24] J.-B. Koo, N. Jiang, S. Saravanamurugan, M. Bejblová, Z. Musilová, J. Čejka, S.-E. Park, *J. Catal.* **2010**, *276*, 327-334.

[25] K. Wang, R. C. Brown, *Green Chem.* **2013**, *15*, 675-681.

Entry for the Table of Contents

FULL PAPER

Playing nice: The interplay of zeolite structural characteristics is studied to identify parameters common to high-performance catalysts in catalytic fast pyrolysis. Crystallinity and accessibility to framework Al atoms was found to be critical to achieve high aromatic yields. These findings allowed us to synthesize a ZSM-5 catalyst with enhanced catalytic properties, offering the highest aromatic hydrocarbon yield reported to date.

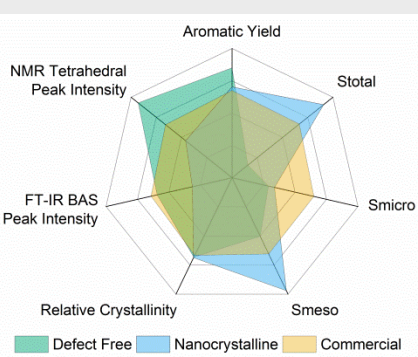

*Thomas C. Hoff, David W. Gardner, Rajeeva Thilakaratne, Kaige Wang, Thomas W. Hansen, Robert C. Brown, and Jean-Philippe Tessonnier**

Page No. – Page No.

Tailoring ZSM-5 Zeolites for the Fast Pyrolysis of Biomass to Aromatic Hydrocarbons